

# APPARENT RESISTIVITY DATA MODELING FOR STANDARD AND ULTRA-LONG ELECTRICAL LOGGING DEVICES

BOGDAN MIHAI NICULESCU

*University of Bucharest, Faculty of Geology and Geophysics, Department of Geophysics  
6 Traian Vuia Street, 020956 Bucharest, Romania  
E-mail: bogdanmihai.niculescu@g.unibuc.ro; bogdan.niculescu@hotmail.com*

*Simulation des diagraphies théoriques de résistivité apparente pour les dispositifs conventionnels et ultra-long de carottage électrique. Les systèmes ULSEL (Ultra-Long Spaced Electrical Logs) sont des dispositifs de carottage électrique de type Normal, à très longs espacements, utilisés pour l'investigation des anomalies résistives ou conductrices éloignées par rapport à la position d'un sondage. Ce genre d'investigations électriques est aussi utilisé pour guider le forage des puits d'intervention, en estimant la distance entre eux et un sondage en éruption, afin de l'intercepter et d'arrêter l'éruption. Les interprétations quantitatives des résultats d'ULSEL, comme les estimations de distance, sont réalisés en comparant la diagraphie de résistivité apparente enregistrée avec la réponse théorique d'un modèle géoélectrique représentatif pour les formations traversées par le trou de sonde. L'article présente un algorithme qui peut être utilisé pour simuler cette réponse, pas seulement pour ULSEL, mais aussi pour les dispositifs conventionnels de carottage électrique, de type Normal et Latéral.*

*Key words:* apparent resistivity, forward modeling, blown-out well, relief well, ULSEL.

## 1. INTRODUCTION

As in the case of surface electrical prospecting, the forward and inverse modeling plays an important role in borehole geophysics. Electrical modeling's field of applicability is represented by the theoretical response simulation of apparent resistivity logging tools in the presence of a geoelectrical model which is representative for the formations crossed by the borehole and, also, by the determination of some physical and dimensional parameters for these formations (layer resistivities, thicknesses and interfaces). In the specific conditions of mud filtrate invasion upon porous-permeable formations, electrical modeling can be used to quantitatively evaluate this process and to determine key parameters involved in the interpretation and evaluation of the productive potential: true resistivity, invaded zone's resistivity and invasion's diameter.

An important application of the forward electrical modeling is related to measurements carried out with ultra-long investigation devices (ULSEL – *Ultra-Long Spaced Electrical Log*). These are Normal devices with very large radii of investigation, used to identify resistive or conductive anomalies located in the proximity of a borehole, such as salt domes, massive reef structures, faults and fractures, metallic casings, etc. This type of electrical surveys may also be used to control the drilling of relief wells, in order to intercept a blown-out well and terminate the eruption (Runge *et al.*, 1969; Runge & Hill, 1971; Mitchell *et al.*, 1972; Haanschoten, 1977). ULSEL is run to insure that the relief well and the target well are sufficiently close to establish communications in the blowout zones and, sometimes, to determine the distance between the wells. Evidently, the presence of a conductive metallic casing within the investigation radius of an ultra-long electrical device will determine a decrease of the recorded apparent resistivity. This effect becomes more important if the investigation device gets closer to the cased well, thus allowing distance estimations and trajectory corrections for a relief well.

Quantitative interpretations of ULSEL results, such as distance estimations, are done by comparing the apparent resistivity log actually recorded with the theoretical response of a layered geoelectrical model that should properly describe the formations intercepted by the target and relief wells.

## 2. FUNDAMENTALS OF ULSEL INVESTIGATION

ULSEL investigations are carried out using Normal devices, with the electrodes A, M and N placed in a borehole and the current-return electrode B located at the surface. Long ULSEL devices usually have electrode spacings of  $AM = 600 / AN = 2400$  ft,  $AM = 1000 / AN = 2400$  ft or  $AM = 1000 / AN = 4000$  ft, while short ULSEL devices frequently use  $AM = 75 / AN = 600$  ft,  $AM = 150 / AN = 600$  ft or  $AM = 150 / AN = 1000$  ft spacings. Recorded apparent resistivity data are not corrected for borehole or mud filtrate invasion effects, due to the very large radii of investigation. Therefore, it is important to emphasize that theoretical ULSEL responses can be computed without taking into account the disturbing factors (mud resistivity and mud filtrate invasion) that affect electrical investigations accomplished with conventional devices.

Interpretation of ULSEL data is performed taking into account the theoretical response of the investigation device in the absence of any lateral resistivity variations. Usually, ULSEL responses are computed using a multilayered geoelectrical model, bounded by homogeneous half-spaces. The number of layers used for the model may reach several hundreds, but one should take into consideration the computation speed and efficiency for the theoretical ULSEL apparent resistivity curve.

The elaboration of the multilayered geoelectrical model is usually carried out using the apparent conductivity curves recorded with induction logging devices (IES – *Induction Electrical Survey*, DIL – *Dual Induction Log* or the modern AIT – *Array Induction Imager Tool*). The apparent conductivity curve, continuously recorded between a borehole's deepest casing level and its maximum depth level, is sampled and processed in order to define a geoelectrical model which adequately represents the geological formations. Such a model may be constructed by analyzing the apparent conductivity curve, selecting the interfaces between the layers using the electrical reflection coefficients (conductivity contrasts) and selecting average conductivity values for the individual layers. In practice, a specialized software is used, which automatically picks up as interfaces the depth levels characterized by a maximum probability of separating layers, averages the conductivities between the interfaces and reciprocates them, in order to define unique values of resistivity for each layer.

Generally, the layered geoelectrical model needs to be extended on a depth interval of minimum 2000 ft above the ULSEL investigated interval, to compensate the effect of resistivity variations upon the N electrode of the device. In practice, the model is enlarged upward and downward with respect to the investigated interval, being delimited by half-spaces with constant resistivity values.

The electrical current distribution in three-dimensional homogeneous and isotropic media is governed by the Laplace equation  $\nabla^2 V = 0$ , where  $V(x, y, z)$  represents the electrical field's potential. Taking into consideration a multilayered geoelectrical model with planar and parallel separation interfaces, the potential function  $V$  may be determined by integrating the Laplace equation in a cylindrical coordinates system  $r, z, \Psi$  ( $r$  – radial distance,  $z$  – vertical distance,  $\Psi$  – azimuthal angle), centered in the source electrode A, and by imposing certain boundary conditions regarding the potential's behavior near the source electrode, at infinity and on the separation interfaces.

A multilayered geoelectrical model with planar-parallel interfaces (Fig. 1) is well-suited for describing geological formations of different thicknesses and resistivities, crossed by boreholes with negligible diameter. The determination of multilayered model's response is accomplished by computing the electrical field's potentials at the depth levels of M and N measurement electrodes, determining consequently the theoretical apparent resistivity. In principle, the method involves finding a solution for the Laplace equation in each layer of the model, subject to proper boundary conditions for each of the separation interfaces (continuity of electrical field's potentials and continuity of the normal component of current's density). All electrodes are assumed to be punctual and the current-return electrode B is considered located at infinity. Also, the first and last layers of the model are assumed to be infinitely extended. In cylindrical coordinates, if  $N$  stands for the number of separation

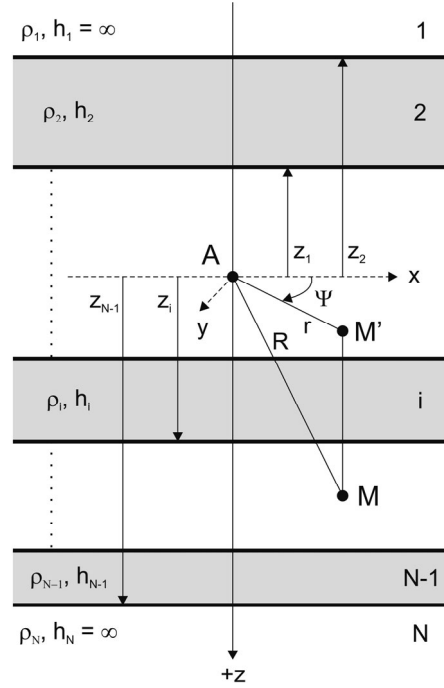


Fig. 1 – Multilayered terrain with planar-parallel separation interfaces and the definition of cylindrical coordinates system. A – source electrode; M – measurement electrode; M' – projection of M on the Axy plane;  $\rho_i, h_i$  – resistivities and thicknesses of the layers.

interfaces, the problem's solution leads to solving a system of  $2N$  linear equations with  $2N$  unknowns („the fundamental system of boundary conditions”) and determining the kernel coefficients  $a_j$  and  $b_j$  which appear in the integral expression of the potential

$$V_M = \frac{I\rho_i}{4\pi} \int_0^{\infty} (a_j(\lambda)e^{-\lambda z} + b_j(\lambda)e^{\lambda z}) J_0(\lambda r) d\lambda, \quad (1)$$

where  $V_M$  represents the potential of the electrical field at electrode M, located at a depth  $z$  within layer  $j$  and at a radial distance  $r$  with respect to the borehole's axis.  $I$  denotes the intensity of the current emitted by the source electrode A,  $\rho_i$  is the electrical resistivity of layer  $i$  and  $J_0(\lambda r)$  is the Bessel function of the first kind and zero order. If the electrode M is placed along borehole's axis, as usually,  $r = 0$  and consequently  $J_0(\lambda r) = 1$ , so

$$V_M = \frac{I\rho_i}{4\pi} \int_0^{\infty} (a_j(\lambda)e^{-\lambda z} + b_j(\lambda)e^{\lambda z}) d\lambda. \quad (2)$$

If  $L = z_{AM}$  stands for the length of the Normal device (taken positive if the electrode M is located below electrode A and negative in the opposite situation), the apparent resistivity measured by the device may be deduced as

$$\rho_A = \frac{4\pi L}{I} V_M = \rho_i L \int_0^{\infty} (a_j(\lambda)e^{-\lambda(\pm L)} + b_j(\lambda)e^{\lambda(\pm L)}) d\lambda. \quad (3)$$

Similar considerations are used in order to compute the theoretical apparent resistivity response for three electrodes AMN devices (Normal and Lateral), taking into consideration the voltage difference  $\Delta V = V_M - V_N$  between the measurement electrodes. From a numerical viewpoint, it should be mentioned that the fundamental system of boundary conditions/equations is continuously changing

along with the movement of source electrode A, due to the placement of A in layers with different resistivities and the variation of distances with respect to the separation interfaces.

For the particular case of ULSEL logs, interpretation is based upon the elaboration of a suitable layered geoelectrical model, computation of the theoretical apparent resistivity response of this model and analysis of the resistivity ratio

$$R = \text{Measured ULSEL resistivity} / \text{Theoretical ULSEL resistivity}. \quad (4)$$

If the ratio deviates from 1, a resistive or conductive anomaly is located in the vicinity of the investigated borehole. The absence of important electrical anomalies in the volume investigated by the ULSEL device is indicated by the random oscillation of one apparent resistivity curve around the other. For relatively simple layered media, the two apparent resistivity curves may be almost superimposed.

Theoretical solutions for the interpretation of apparent resistivity data corresponding to layered media, neglecting the borehole effects, have been proposed by Dahnov (1961), Van Nostrand & Cook (1966), Daniels (1978) and Yang & Ward (1984). The Laplace equation is solved analytically, in cylindrical coordinates, and sometimes a recursive procedure is employed in order to determine the kernel coefficients  $a(\lambda)$  and  $b(\lambda)$ . For the purpose of this study, a combined analytical-numerical treatment of the problem was used, by means of an original algorithm and software (Niculescu, 2002, 2006) applicable for both ideal (AM) and real (AMN) electrode arrays placed in multilayered media. The algorithm builds the fundamental system of boundary conditions for each successive position of the electrodes, then the system is solved numerically (via a fast Gaussian elimination procedure) for the kernel coefficients  $a(\lambda)$  and  $b(\lambda)$ , while iteratively incrementing the arbitrary integration variable  $\lambda$  with a sufficiently small step  $d\lambda$ . During the same process of  $\lambda$  incrementation, until convergence is achieved, the potentials of M and N electrodes are computed by means of a first or second degree numerical integration procedure and the apparent resistivity is determined for each depth sampling level.

### 3. DESCRIPTION OF THE PROPOSED ALGORITHM

As stated previously, for the forward modeling of multistratified media electrical response the Laplace differential equation was used, its expression in a Cartesian  $(x, y, z)$  coordinates system being

$$\frac{\partial^2 V}{\partial x^2} + \frac{\partial^2 V}{\partial y^2} + \frac{\partial^2 V}{\partial z^2} = 0. \quad (5)$$

Using a cylindrical  $(r, z, \Psi)$  coordinates system centered in the source electrode A and taking into consideration the electrical field potential's symmetry around the vertical  $z$  axis, equation (5) becomes

$$\frac{\partial^2 V}{\partial r^2} + \frac{1}{r} \frac{\partial V}{\partial r} + \frac{\partial^2 V}{\partial z^2} = 0. \quad (6)$$

The Bessel functions method (Sabba Ștefănescu, 1930) allows expressing the solution of the differential equation (6) through a potential function

$$v(r, z) = (a(\lambda)e^{-\lambda z} + b(\lambda)e^{\lambda z})J_0(\lambda r), \quad (7)$$

where the kernel coefficients  $a(\lambda)$  and  $b(\lambda)$  are determined taking into account the particular conditions of the problem,  $J_0(\lambda r)$  is the Bessel function of the first kind and zero order and  $\lambda$  is an arbitrary variable. In order to simplify the notation,  $a = a(\lambda)$  and  $b = b(\lambda)$  symbols will be used henceforth.

Considering the Weber-Lipschitz integral identity

$$\int_0^{\infty} e^{-\lambda z} J_0(\lambda r) d\lambda = \frac{1}{\sqrt{r^2 + z^2}} = \frac{1}{R}, \quad (8)$$

one may observe that the normal potential within a homogeneous and isotropic medium

$$V = \frac{I\rho}{4\pi} \cdot \frac{1}{R} \quad (9)$$

may be considered as the sum (integral) of several elementary potentials expressed by

$$v_0(r, z) = e^{-\lambda z} J_0(\lambda r) \quad (10)$$

and multiplied with the constant factor  $I\rho/4\pi$ . Because the potential  $v_0$  has to be finite in every point of the medium and should cancel at infinity (for  $z \rightarrow \pm \infty$ ), the following formal notation will be adopted:

$$v_0 = e^{-\lambda|z|} J_0(\lambda r) \quad (11)$$

to eliminate the  $z$  vertical distances sign variations. In the previous equations,  $I$  stands for the current intensity,  $\rho$  represents the medium's resistivity,  $r$  is the radial distance between the potential electrode M and the borehole's axis,  $z$  denotes a vertical distance between the A and M electrodes or between A and the separation interfaces and  $R$  represents the effective distance between said electrodes.

The algorithm's objective is to determine the response of a multilayered geoelectrical model subject to an excitation potential  $v_0$ , by evidencing the elementary potentials which appear within each of the model's layers. The elementary potentials thus determined are integrated and multiplied with  $I\rho/4\pi$  type quantities, in order to determine the electrical field's potentials  $V$  for each layer.

Figure 2 shows a multilayered geoelectrical model with  $N$  planar-parallel and horizontal interfaces, separating  $N+1$  homogeneous and isotropic layers with different thicknesses and resistivities. The first and last (1 and  $N+1$ ) layers of the model are assumed infinitely extended and the  $z$  axis of the cylindrical coordinates system is considered normal to the separation interfaces and positive in the downward direction. The source electrode A is considered located in an arbitrary layer  $i$  and the potential electrode M in an arbitrary layer  $j$ . The quantities  $z_k$  ( $k = 1, \dots, N$ ) are the vertical distances between electrode A and the interfaces,  $z_k$  being positive or negative depending upon the position of A.

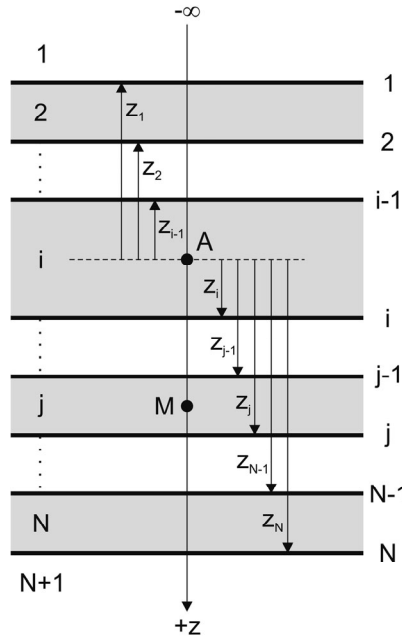


Fig. 2 – Normal AM device located in a multilayered terrain, with  $N$  separation interfaces and  $N+1$  homogeneous and isotropic layers. The source electrode A is located in an arbitrary layer  $i$ , the measurement electrode M in an arbitrary layer  $j$  and  $z_k$  ( $k = 1, \dots, N$ ) are the vertical distances between A and the interfaces.

The determination of model's response in terms of apparent resistivity demands, as a first step, the elaboration of the fundamental system of boundary conditions. For  $N$  separation interfaces,  $2N$  boundary conditions are necessary (continuity of electrical field's potentials and continuity of the normal component of current's density, across each interface) and it should be pointed out that the system's structure is continuously changing, due to the successive positions of source electrode A and variable distances between A and the separation interfaces. Taking into consideration an arbitrary interface  $i$  between two layers with resistivities  $\rho_i$  and  $\rho_{i+1}$ , the boundary conditions can be expressed as

$$v_i \Big|_{z=\pm z_i} = v_{i+1} \Big|_{z=\pm z_i} \quad (12)$$

$$\frac{1}{\rho_i} \frac{\partial v_i}{\partial z} \Big|_{z=\pm z_i} = \frac{1}{\rho_{i+1}} \frac{\partial v_{i+1}}{\partial z} \Big|_{z=\pm z_i}, \quad (13)$$

according to the sign of the vertical distances between A and the interface ( $z_i > 0$ , if A is located above the interface, and  $z_i < 0$ , if A is located below the interface).

Boundary conditions are actually constructed by analyzing two different situations for the arbitrary interface  $i$ : the placement of source electrode A in the vicinity of the interface (in layers  $i$  or  $i+1$ ), or the positioning of A in other layers than the ones adjacent to the interface. The general expression for the electrical field's elementary potential in an arbitrary layer  $i$  is

$$v_i = (a_i e^{-\lambda z} + b_i e^{\lambda z}) J_0(\lambda r) \quad (14)$$

and if source electrode A is located in the same layer, a normal excitation potential  $v_0$  given by (11) is added to the elementary potential  $v_i$ , such that

$$v_i = (e^{-\lambda|z|} + a_i e^{-\lambda z} + b_i e^{\lambda z}) J_0(\lambda r). \quad (15)$$

For the multilayered geoelectrical model taken into consideration, the fundamental system of boundary conditions may be expressed in matrix notation as

$$\mathbf{M} \mathbf{x} = \mathbf{v}, \quad (16)$$

where:

- $\mathbf{M}$  = square system matrix with  $[2N \times 2N]$  dimension, storing coefficients (of  $\pm e^{\pm \lambda z}$  and  $\pm \rho e^{\pm \lambda z}$  form) for the unknown kernel terms  $a_i$  and  $b_i$ ;
- $\mathbf{x}$  = column vector with  $[2N \times 1]$  dimension, storing the unknown kernel terms  $a_i$  and  $b_i$ ;
- $\mathbf{v}$  = column vector with  $[2N \times 1]$  dimension, storing the free terms of the system.

In the system matrix  $\mathbf{M}$  and the free terms vector  $\mathbf{v}$  two rows are reserved for each separation interface, in agreement with the necessary boundary conditions. For an arbitrary interface  $i$ , the elements of the corresponding rows are:

- If the source electrode A is not located in layers  $i$  or  $i+1$  and the distance  $z_i$  to the separation interface is positive (Fig. 3a), then

$$\begin{bmatrix} \cdot & \cdot & \cdot & \cdot & \cdot & \cdot \\ \cdot & \cdot & \cdot & \cdot & \cdot & \cdot \\ \cdot & e^{-\lambda z_i} & e^{\lambda z_i} & -e^{-\lambda z_i} & -e^{\lambda z_i} & \cdot \\ \cdot & -\rho_{i+1} e^{-\lambda z_i} & \rho_{i+1} e^{\lambda z_i} & \rho_i e^{-\lambda z_i} & -\rho_i e^{\lambda z_i} & \cdot \\ \cdot & \cdot & \cdot & \cdot & \cdot & \cdot \\ \cdot & \cdot & \cdot & \cdot & \cdot & \cdot \end{bmatrix} \begin{bmatrix} \cdot \\ \cdot \\ a_i \\ b_i \\ a_{i+1} \\ b_{i+1} \\ \cdot \\ \cdot \end{bmatrix} = \begin{bmatrix} \cdot \\ \cdot \\ 0 \\ 0 \\ \cdot \\ \cdot \\ \cdot \\ \cdot \end{bmatrix}; \quad (17)$$

$\mathbf{M} \qquad \mathbf{x} \qquad \mathbf{v}$

- If the source electrode A is not located in layers  $i$  or  $i+1$  and the distance  $z_i$  to the separation interface is negative (Fig. 3a), then

$$\begin{bmatrix} \cdot & \cdot & \cdot & \cdot & \cdot & \cdot \\ \cdot & \cdot & \cdot & \cdot & \cdot & \cdot \\ \cdot & e^{\lambda z_i} & e^{-\lambda z_i} & -e^{\lambda z_i} & -e^{-\lambda z_i} & \cdot \\ \cdot & \rho_{i+1} e^{\lambda z_i} & -\rho_{i+1} e^{-\lambda z_i} & -\rho_i e^{\lambda z_i} & \rho_i e^{-\lambda z_i} & \cdot \\ \cdot & \cdot & \cdot & \cdot & \cdot & \cdot \\ \cdot & \cdot & \cdot & \cdot & \cdot & \cdot \end{bmatrix} \begin{bmatrix} \cdot \\ \cdot \\ a_i \\ b_i \\ a_{i+1} \\ b_{i+1} \\ \cdot \\ \cdot \end{bmatrix} = \begin{bmatrix} \cdot \\ \cdot \\ 0 \\ 0 \\ \cdot \\ \cdot \end{bmatrix}; \quad (18)$$

**M** **x** **v**

- If the source electrode A is located in layer  $i$  (above the  $i$  separation interface) and the distance  $z_i$  to the interface is positive (Fig. 3b), then

$$\begin{bmatrix} \cdot & \cdot & \cdot & \cdot & \cdot & \cdot \\ \cdot & \cdot & \cdot & \cdot & \cdot & \cdot \\ \cdot & e^{-\lambda z_i} & e^{\lambda z_i} & -e^{-\lambda z_i} & -e^{\lambda z_i} & \cdot \\ \cdot & -\rho_{i+1} e^{-\lambda z_i} & \rho_{i+1} e^{\lambda z_i} & \rho_i e^{-\lambda z_i} & -\rho_i e^{\lambda z_i} & \cdot \\ \cdot & \cdot & \cdot & \cdot & \cdot & \cdot \\ \cdot & \cdot & \cdot & \cdot & \cdot & \cdot \end{bmatrix} \begin{bmatrix} \cdot \\ \cdot \\ a_i \\ b_i \\ a_{i+1} \\ b_{i+1} \\ \cdot \\ \cdot \end{bmatrix} = \begin{bmatrix} \cdot \\ \cdot \\ -e^{-\lambda z_i} \\ \rho_{i+1} e^{-\lambda z_i} \\ \cdot \\ \cdot \end{bmatrix}; \quad (19)$$

**M** **x** **v**

- If the source electrode A is located in layer  $i+1$  (below the  $i$  separation interface) and the distance  $z_i$  to the interface is negative (Fig. 3b), then

$$\begin{bmatrix} \cdot & \cdot & \cdot & \cdot & \cdot & \cdot \\ \cdot & \cdot & \cdot & \cdot & \cdot & \cdot \\ \cdot & e^{\lambda z_i} & e^{-\lambda z_i} & -e^{\lambda z_i} & -e^{-\lambda z_i} & \cdot \\ \cdot & \rho_{i+1} e^{\lambda z_i} & -\rho_{i+1} e^{-\lambda z_i} & -\rho_i e^{\lambda z_i} & \rho_i e^{-\lambda z_i} & \cdot \\ \cdot & \cdot & \cdot & \cdot & \cdot & \cdot \\ \cdot & \cdot & \cdot & \cdot & \cdot & \cdot \end{bmatrix} \begin{bmatrix} \cdot \\ \cdot \\ a_i \\ b_i \\ a_{i+1} \\ b_{i+1} \\ \cdot \\ \cdot \end{bmatrix} = \begin{bmatrix} \cdot \\ \cdot \\ e^{-\lambda z_i} \\ -\rho_i e^{-\lambda z_i} \\ \cdot \\ \cdot \end{bmatrix}. \quad (20)$$

**M** **x** **v**

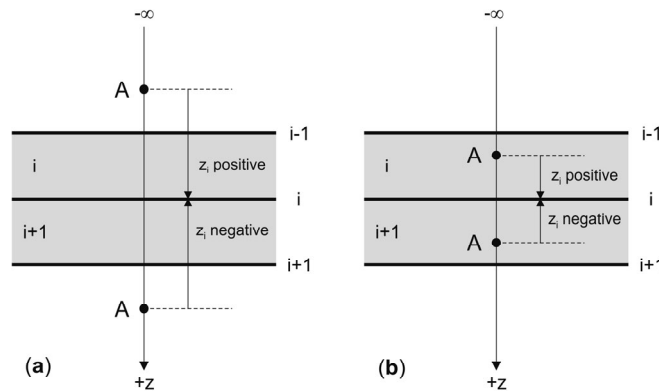


Fig. 3 – a) Source electrode A situated far from an arbitrary interface  $i$ , *i.e.*, not in the adjacent layers  $i$  or  $i+1$ ; b) Source electrode A situated immediately above or below an arbitrary interface  $i$ , in the adjacent layers  $i$  or  $i+1$ .

Special conditions must be imposed for some particular cases related to the position of the source electrode A. If A is located in the layers 1 or  $N+1$  (both infinitely extended), the  $\mathbf{v}$  vector will contain only two non-zero terms, corresponding to the separation interfaces 1 or  $N$ , the remaining free terms being nil. Also, if A is located in an internal layer  $i$ , the  $\mathbf{v}$  vector will contain only four non-zero terms, corresponding to  $i-1$  and  $i$  interfaces.

For better understanding the system of equations (16), its structure will be presented for the simple case of  $N = 3$  separation interfaces. Assuming that layers 1 and  $N+1$  are infinitely extended and considering that the potentials should cancel in these layers, some kernel terms will also cancel ( $a_1 = 0$  and  $b_{N+1} = 0$ ). The system matrix  $\mathbf{M}$  takes the form

$$\mathbf{M} = \begin{matrix} & b_1 & a_2 & b_2 & a_3 & b_3 & a_4 \\ \begin{bmatrix} x & x & x & 0 & 0 & 0 \\ x & x & x & 0 & 0 & 0 \\ 0 & x & x & x & x & 0 \\ 0 & x & x & x & x & 0 \\ 0 & 0 & 0 & x & x & x \\ 0 & 0 & 0 & x & x & x \end{bmatrix} & & & & & & \end{matrix}, \quad (21)$$

where the „ $x$ ” symbols denote non-zero elements of  $\pm e^{\pm\lambda z}$  and  $\pm \rho e^{\pm\lambda z}$  type, disposed along or near the main diagonal. The structure of matrix  $\mathbf{M}$  does not change while the source electrode A is moving along borehole's axis, but the symbolic elements „ $x$ ” values are variable, due to the continuously changing vertical distances  $z_i$ . The system (16) and the free terms vector  $\mathbf{v}$  can be expressed as

$$\mathbf{M} \begin{bmatrix} b_1 \\ a_2 \\ b_2 \\ a_3 \\ b_3 \\ a_4 \end{bmatrix} = \begin{bmatrix} x \\ x \\ 0 \\ 0 \\ 0 \\ 0 \end{bmatrix} \begin{bmatrix} x \\ x \\ x \\ x \\ 0 \\ 0 \end{bmatrix} \begin{bmatrix} x \\ x \\ x \\ x \\ x \\ x \end{bmatrix} \begin{bmatrix} 0 \\ 0 \\ x \\ x \\ x \\ x \end{bmatrix} \begin{bmatrix} 0 \\ 0 \\ 0 \\ x \\ x \\ x \end{bmatrix}, \quad (22)$$

$\mathbf{x} \qquad \mathbf{v}_1 \qquad \mathbf{v}_2 \qquad \mathbf{v}_3 \qquad \mathbf{v}_4$

the  $\mathbf{v}$  vectors above corresponding to the placement of electrode A in the layers 1, 2, 3 and 4.

The fundamental system of boundary conditions (16) may be solved numerically for the kernel coefficients  $b_1, a_2, b_2, \dots, a_N, b_N$  and  $a_{N+1}$ , using an adequate procedure (direct methods – Gauss, Gauss-Jordan or iterative methods – Jacobi, Gauss-Seidel, successive over-relaxation, etc.). In this study, a solver based on Gaussian elimination with partial pivoting was elaborated and used, in order to avoid division by zero problems and to reduce the round-off errors. It is important to point out that a computationally efficient numerical procedure should be employed, because the fundamental system of boundary conditions is solved for the  $2N$  unknowns in each successive position of the electrodes.

Once the kernel coefficients are determined, the electrical field's potentials and the corresponding theoretical apparent resistivities may be computed for any AM or AMN investigation devices (Fig. 4), using a first or second degree numerical integration method. For an AM device moving along a borehole's axis, taking into account that the radial distance is  $r_{AM} = 0$  and  $J_0(\lambda r_{AM}) = 1$ , it can be shown that the potential  $V_M$  is

$$V_M = \frac{I\rho_i}{4\pi} \int_0^{\infty} (a_j e^{-\lambda(\pm L)} + b_j e^{\lambda(\pm L)}) d\lambda \quad (23)$$

(if electrode A is located in an arbitrary layer  $i$  and electrode M in an arbitrary layer  $j$ )

$$V_M = \frac{I\rho_i}{4\pi} \left[ \frac{1}{L} + \int_0^{\infty} (a_i e^{-\lambda(\pm L)} + b_i e^{\lambda(\pm L)}) d\lambda \right] \quad (24)$$

(if both A and M electrodes are located in the same arbitrary layer  $i$ ),

where  $L = z_{AM}$  represents the device's length (considered positive if M is located below A and negative in the opposite situation). The apparent resistivity measured by the device will be

$$\rho_A = \frac{4\pi L}{I} V_M = \rho_i L \int_0^{\infty} (a_j e^{-\lambda(\pm L)} + b_j e^{\lambda(\pm L)}) d\lambda \quad (25)$$

(if electrode A is located in an arbitrary layer  $i$  and electrode M in an arbitrary layer  $j$ )

$$\rho_A = \frac{4\pi L}{I} V_M = \rho_i \left[ 1 + L \int_0^{\infty} (a_i e^{-\lambda(\pm L)} + b_i e^{\lambda(\pm L)}) d\lambda \right] \quad (26)$$

(if both A and M electrodes are located in the same arbitrary layer  $i$ ).

Same method is employed to determine the theoretical apparent resistivity response for three electrodes AMN devices, by computing the potentials  $V_M$  and  $V_N$  and considering the device's geometric factor,  $\rho_A$  being referenced at a conventional midpoint O between the M and N measurement electrodes:

$$\rho_A = 4\pi \frac{AM \ AN}{MN} \cdot \frac{V_M - V_N}{I} \quad (27)$$

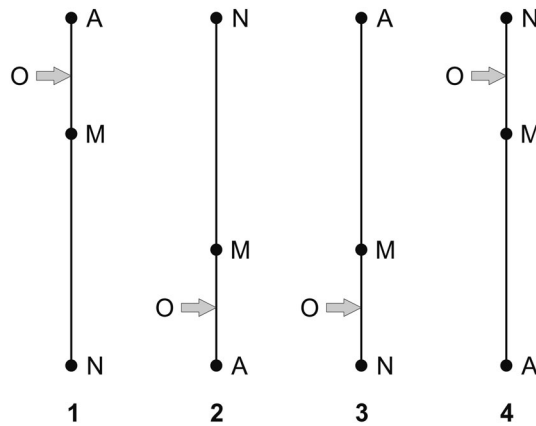


Fig. 4 – Three electrodes AMN devices used in the forward modeling algorithm: 1 – consecutive Normal device; 2 – non-consecutive Normal device; 3 – consecutive Lateral device; 4 – non-consecutive Lateral device. A – source electrode; M, N – measurement electrodes; O – apparent resistivity reference point. The current-return electrode B is assumed to be located at the surface (at infinity).

The numerical integration procedures implemented and employed in this study are performed iteratively, with a sufficiently small step  $d\lambda$  and precision  $\varepsilon$  (absolute difference between the values of the potentials  $V$  in two successive iterations), both imposed by the user, until convergence is achieved at each computation depth level. Generally, the slowest rate of convergence occurs in the neighborhood of the separation interfaces and the electrical modeling is more computationally-intensive in the case of thick layers, while the thin layers response is simulated much faster. Figure 5 shows the computed theoretical effect and the corresponding number of numerical integration iterations for a Normal AM device ( $N \rightarrow \infty$ ) and a simple model representing a thick resistive layer (ratio  $AM/h = 0.1$ , where  $h$  is the layer's thickness). The simulation was carried out using a quadratic (Simpson's rule) integration procedure, with an integration step  $d\lambda = 10^{-3}$  and a precision  $\varepsilon = 10^{-6}$ .

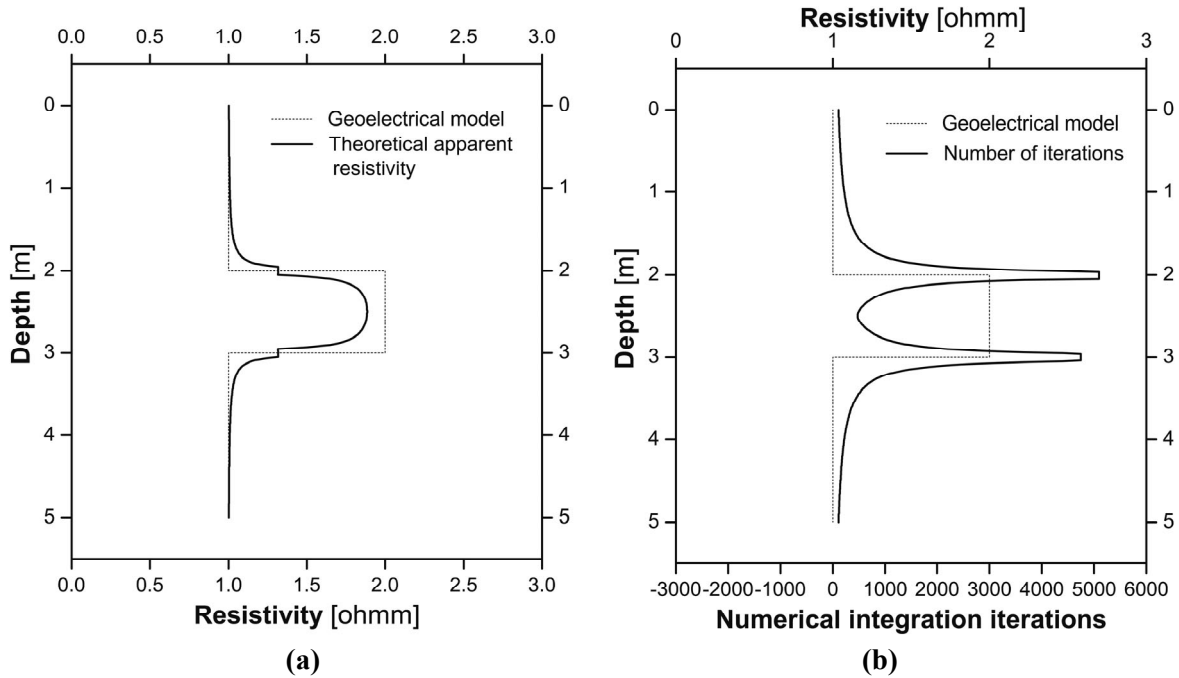


Fig. 5 – a) Theoretical apparent resistivity response of a Normal AM device ( $L = AM = 0.1$  m;  $N \rightarrow \infty$ ) for a thick ( $h = 1$  m) resistive layer; b) Number of numerical integration iterations required to compute the apparent resistivity response.

#### 4. RESULTS AND CONCLUSIONS

Figures 6 and 7 illustrate the practical applicability of the described forward modeling algorithm, by simulating the apparent resistivity response of Normal AM ( $L = AM = 1$  m) and Lateral AMN ( $L = AO = 1$  m,  $MN = 10^{-3}$  m) electrode arrays for a rather complicated geoelectrical model with 9 layers ( $\rho_1 = 10 \Omega\text{m}$ ,  $\rho_2 = 100 \Omega\text{m}$ ,  $\rho_3 = 10 \Omega\text{m}$ ,  $\rho_4 = 1 \Omega\text{m}$ ,  $\rho_5 = 10 \Omega\text{m}$ ,  $\rho_6 = 100 \Omega\text{m}$ ,  $\rho_7 = 10 \Omega\text{m}$ ,  $\rho_8 = 1 \Omega\text{m}$ ,  $\rho_9 = 10 \Omega\text{m}$ ;  $h_1 \rightarrow \infty$ ,  $h_2 = 1$  m,  $h_3 = 2$  m,  $h_4 = 1$  m,  $h_5 = 2$  m,  $h_6 = 4$  m,  $h_7 = 2$  m,  $h_8 = 4$  m,  $h_9 \rightarrow \infty$ ). The simulation's parameters are: numerical integration method = quadratic; numerical integration step  $d\lambda = 10^{-3}$ ; numerical integration precision  $\varepsilon = 10^{-6}$ ; depth sampling step  $\Delta h = 0.05$  m (401 computation levels on a 20 m depth interval). One may easily notice the complexity of the theoretical apparent resistivity responses, the presence of thin layer effects, as well as blind zones and reflection peaks for the Lateral array.

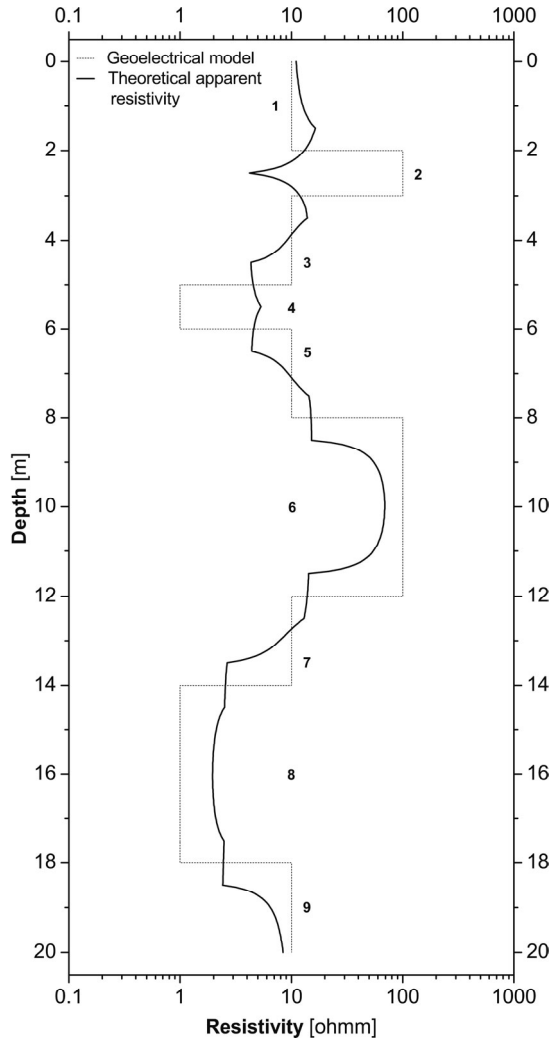


Fig. 6 – Theoretical apparent resistivity response of a Normal AM device ( $L = AM = 1$  m;  $N \rightarrow \infty$ ) for a complex multilayered geoelectrical model.

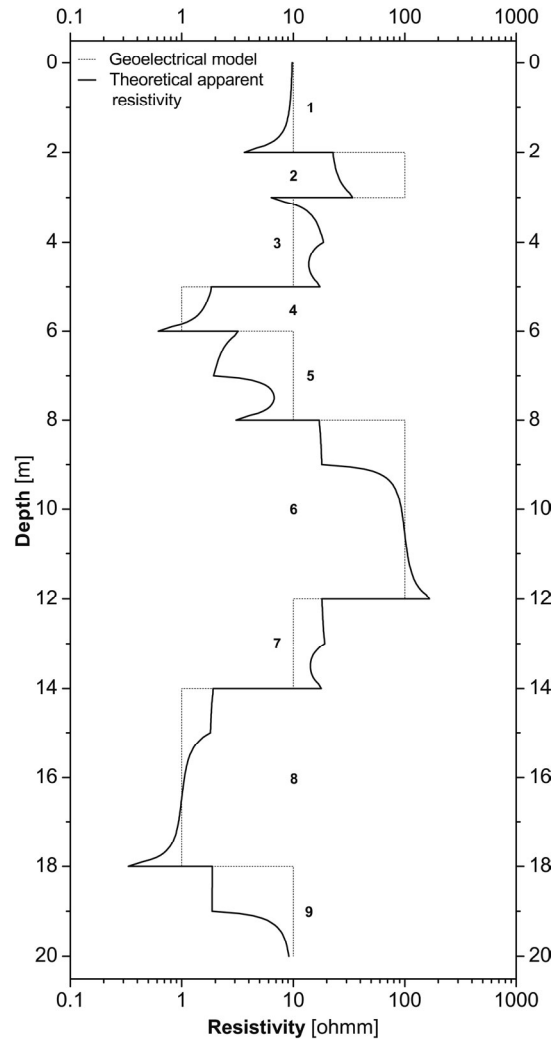


Fig. 7 – Theoretical apparent resistivity response of a Lateral AMN device ( $L = AO = 1$  m;  $MN \rightarrow 0$ ) for a complex multilayered geoelectrical model.

Figures 8 and 9 show a simulation of the apparent resistivity response for the short (75/600 ft, 150/600 ft, 150/1000 ft) and long (600/2400 ft, 1000/2400 ft, 1000/4000 ft) ULSEL devices and a 9 layers geoelectrical model ( $\rho_1 = 10 \Omega\text{m}$ ,  $\rho_2 = 100 \Omega\text{m}$ ,  $\rho_3 = 10 \Omega\text{m}$ ,  $\rho_4 = 1 \Omega\text{m}$ ,  $\rho_5 = 10 \Omega\text{m}$ ,  $\rho_6 = 100 \Omega\text{m}$ ,  $\rho_7 = 10 \Omega\text{m}$ ,  $\rho_8 = 1 \Omega\text{m}$ ,  $\rho_9 = 10 \Omega\text{m}$ ;  $h_1 \rightarrow \infty$ ,  $h_2 = 10$  m,  $h_3 = 20$  m,  $h_4 = 10$  m,  $h_5 = 20$  m,  $h_6 = 40$  m,  $h_7 = 20$  m,  $h_8 = 40$  m,  $h_9 \rightarrow \infty$ ). The parameters used for the simulation are: numerical integration method = quadratic; numerical integration step  $d\lambda = 10^{-3}$ ; numerical integration precision  $\varepsilon = 10^{-6}$ ; depth sampling step  $\Delta h = 0.5$  m (401 computation levels on a 200 m depth interval). As the length of the devices increases, there is a tendency of averaging the geoelectrical model's resistivities and the apparent resistivity curves progressively flatten. The very long ULSEL devices perceive the model as a „thin layer”, their response being an extended minimum, with lack of details on the apparent resistivity curves and a tendency of dropping towards zero. If no electrical modeling were carried out, only by analyzing the actual apparent resistivity curves which would have been recorded with these devices, one may erroneously conclude that the investigated well is close to the conductive metallic casing of a target well.

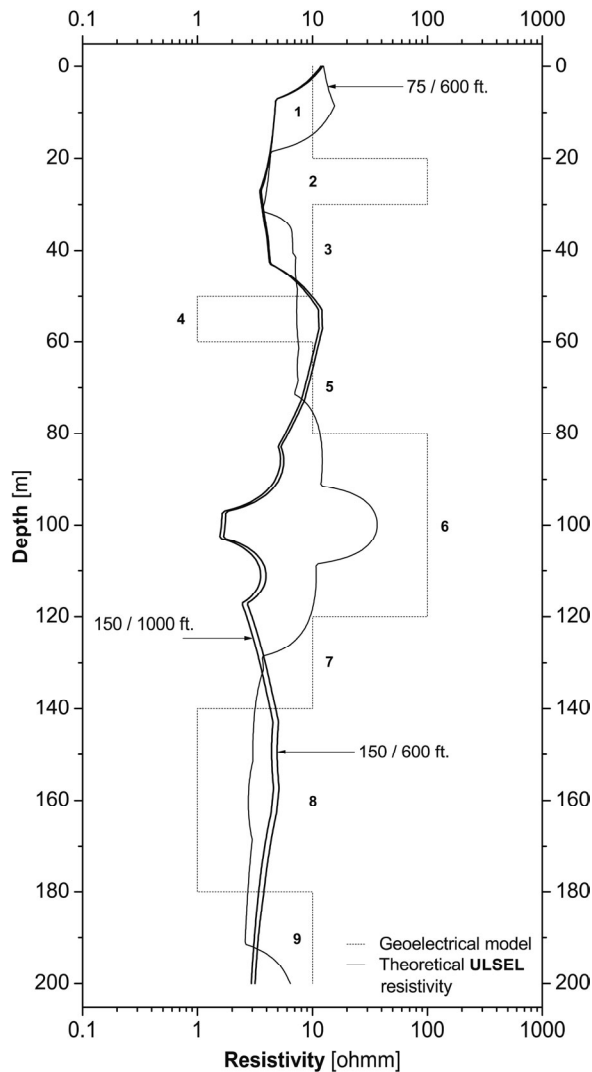


Fig. 8 – Theoretical apparent resistivity responses of short (75/600 ft, 150/600 ft, 150/1000 ft) ULSEL devices for a complex multilayered geoelectrical model.

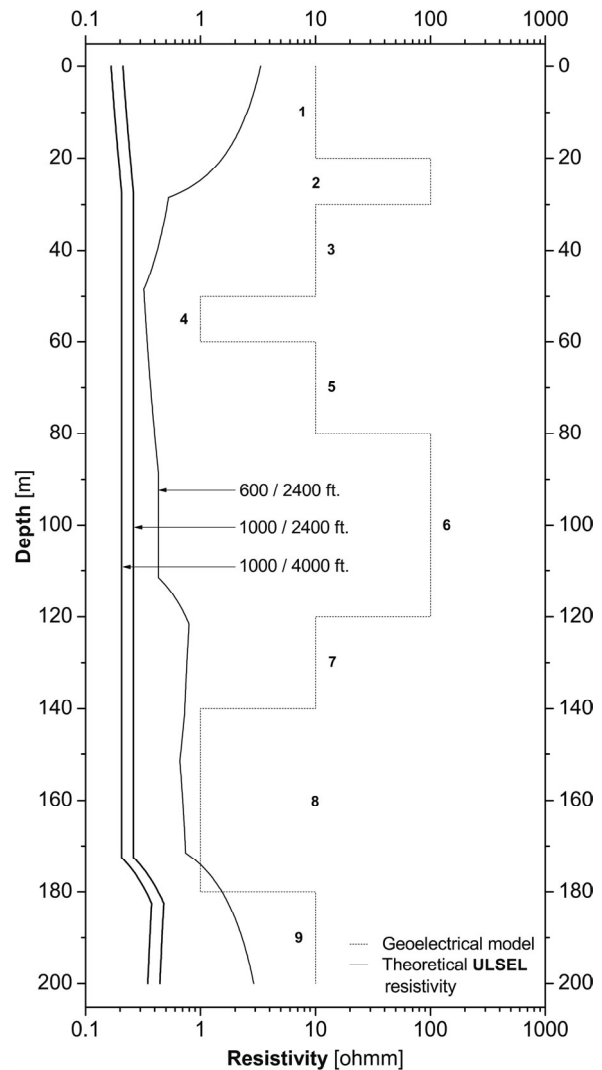


Fig. 9 – Theoretical apparent resistivity responses of long (600/2400 ft, 1000/2400 ft, 1000/4000 ft) ULSEL devices for a complex multilayered geoelectrical model.

The algorithm elaborated and presented is able to simulate the response of any standard or ultra-long electrical investigation arrays for a certain type of multilayered models, with horizontal planar-parallel interfaces and no invasion. Its field of applicability includes theoretical borehole geophysics studies and, also, solving some important technical and economical problems related to the operation of wells.

#### REFERENCES

- DAHNOV, V.N. (1961), *Interpretation of borehole geophysical logging results*, Technical Publishing House, Bucharest (in Romanian).
- DANIELS, J.J. (1978), *Interpretation of buried electrode resistivity data using a layered earth model*, *Geophysics*, **43**, 988–1001.
- HAANSCHOTEN, G.W. (1977), *ULSEL logging in blow-out relief wells*, *The Log Analyst*, **18** (1), 23–32.
- HAANSCHOTEN, G.W. (1977), *ULSEL guides relief wells*, *Oil and Gas Journal*, **75** (2), 70–74.

- MITCHELL, F.R., ROBINSON, J.D., VOGIATZIS, J.P., PEHOUSHEK, F., MORAN, J.H., AUSBURN, B.E., BERRY, L.N. (1972), *Determination of distance between wells utilizing resistivity measurements*, Journal of Petroleum Technology, **24** (6), 723–741.
- NICULESCU, B.M. (2006), *FORWARD ELECTRICAL MODELING – Applications in borehole geophysics*, University of Bucharest Publishing House, Bucharest (in Romanian), 214 pp., ISBN 973-737-161-5.
- NICULESCU, B.M. (2002), *Contributions to the electrical modeling of stratified media. Specific applications in borehole geophysics*, Ph.D. Thesis, University of Bucharest, Bucharest (in Romanian), 355 pp..
- RUNGE, R.J., WORTHINGTON, A.E., LUCAS, D.R. (1969), *Ultra-Long Spaced Electrical Log (ULSEL)*, S.P.W.L.A. Transactions, 10th Annual Logging Symposium, Houston, U.S.A., H1-H22, 1969.
- RUNGE, R.J., HILL, D.G. (1971), *The role of anisotropy in ULSEL*, S.P.W.L.A. Transactions, 12th Annual Logging Symposium, Dallas, U.S.A., J1-J23, 1971.
- ȘTEFĂNESCU, Sabba S. (1930), *Sur la distribution électrique potentielle autour d'une prise de terre ponctuelle dans un terrain à couches horizontales, homogènes et isotropes*, Journal de Physique et le Radium, **7** (1), 132–140.
- VAN NOSTRAND, R.G., COOK, K.L. (1966), *Interpretation of resistivity data*, U.S. Geological Survey Professional Paper, No. **499**.
- YANG, F.W., WARD, S.H. (1984), *Inversion of borehole normal resistivity logs*, Geophysics, **49** (9), 1541–1548.

Received: July, 2008

Accepted for publication: October, 2008

